Accepted Manuscript

Effect of starch reduced graphene oxide on thermal and mechanical properties of phenol formaldehyde resin nanocomposites

P.K. Sandhya, M.S. Sreekala, Moothetty Padmanabhan, K. Jesitha, Sabu Thomas

PII: S1359-8368(18)30917-X

DOI: https://doi.org/10.1016/j.compositesb.2018.12.009

Reference: JCOMB 6338

To appear in: *Composites Part B*

Received Date: 21 March 2018

Revised Date: 25 November 2018

Accepted Date: 3 December 2018

Please cite this article as: Sandhya PK, Sreekala MS, Padmanabhan M, Jesitha K, Thomas S, Effect of starch reduced graphene oxide on thermal and mechanical properties of phenol formaldehyde resin nanocomposites, *Composites Part B* (2019), doi: https://doi.org/10.1016/j.compositesb.2018.12.009.

Effect of Starch Reduced Graphene Oxide on Thermal and Mechanical Properties of Phenol Formaldehyde Resin Nanocomposites

Sandhya P K [a], M S Sreekala [b], Moothetty Padmanabhan[a,c], Jesitha K[b], Sabu Thomas[a]

[a]School of Chemical Sciences, M G University, Kottayam 686560, Kerala, India

[b]Post Graduate Department of Chemistry, Sree Sankara College, Kalady 683574, Kerala, India

[c]Department of Chemistry, Amrita Vishwa Vidyapeetham, Amritapuri, 690525, Kerala, India

ABSTRACT

Phenol formaldehyde (PF) resins are one of the oldest synthesized and very widely used resins. Their properties can be improved with the incorporation nano-fillers even with lower loadings. Graphene materials have attracted significant attention in recent years owing to its exceptional thermal, mechanical and electrical properties. Herein, we report a very simple and effective way to reduce graphene oxide (GO) by using highly abundant potato starch instead of conventionally used toxic and hazardous reducing agents like hydrazine. The reduced GO (RGO) is then effectively incorporated into PF resin by optimizing various processing parameters. The reinforcing effect of RGO sheets on the PF matrix was investigated by X-ray diffraction (XRD) and Transmission Electron Microscopy (TEM). The effect of RGO on thermal properties of the polymer nanocomposites was studied using Thermo Gravimetric Analysis (TGA). The mechanical properties of PF/RGO composites were studied by tensile and Izod impact tests. The fracture mechanism of the composites was investigated by Scanning Electron Microscopy. Theoretical prediction of the mechanical properties of the nanocomposites using Halpin-Tsai models gave sufficient information regarding the orientation of graphene sheets in PF matrix.

***Key words*:** Phenol formaldehyde; potato starch; reduced graphene oxide

Graphical Abstract:

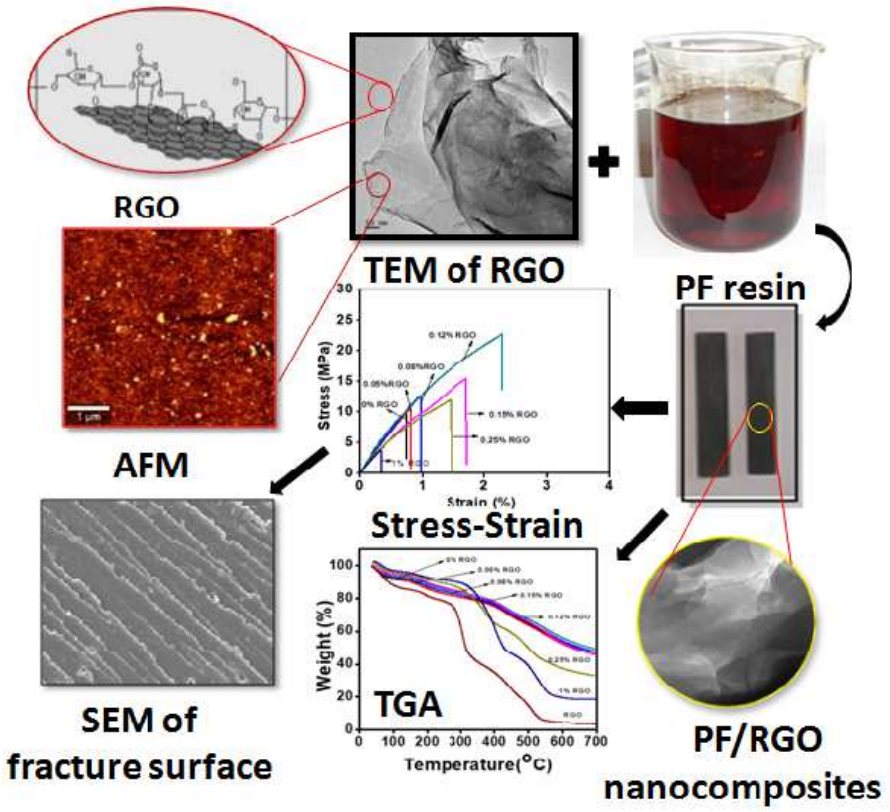

Scheme illustrating formation of PF/RGO nanocomposites

*Corresponding Author address

Email: sabupolymer@yahoo.com

1. Introduction

Phenol formaldehyde (PF) resole resin is one of the oldest synthesized low-cost resins with excellent thermal stability, mechanical properties, good solvent and weather resistance which make them excellent candidate for a wide variety of applications in the fields of thermal insulation, coatings, automotive and aerospace industries. Their FST

(fire, smoke, low toxicity) properties also make them highly favorable for composite preparation [1]. In spite of these advantages only a very few studies have been made on this phenolic resin since it is known to form three-dimensional molecular structure even before it is cured. Phenolics are generally very brittle but that can be modified and varied by adding appropriate fillers or other additives into the matrix.

Graphene is well-known for its excellent mechanical properties such as high tensile strength, high Young's modulus, and fracture toughness but the lack of any reacting functionalities make it non-responsive to any composite formation. However, layered graphene oxide (GO) which we get by exfoliation of graphite possess several surface O-functionalities which can facilitate the interfacial interaction, effective dispersion and hence efficient load transfer between GO layers and the polymer matrix[2]. Therefore, GO can function as an ideal candidate for imparting many of graphene-related properties like superior mechanical, electrical and electronic properties, light weight and the high surface area nature in its nanocomposites making them versatile multifunctional materials [3]. Different methods are used for the synthesis graphene like mechanical exfoliation [4], Chemical Vapour Deposition (CVD) [5], chemical oxidation/ exfoliation followed by reduction of graphene derivatives such as graphene oxide (GO) [6,7], unzipping carbon nanotubes [8], arc discharge methods [9]. Among these methods, chemical oxidation of natural graphite by Hummers method followed by reduction is the most commonly used method. Earlier, the chemical reduction of GO were performed using various reducing agents such as hydrazine and its derivatives [10-16], $NaBH_4$ [17, 18], hydroquinone [19], hydroiodic acid (HI) [20-22], sulfur-containing compounds [23], metal powders [24-27] and hydroxylamine [28]. Among these the most widely adopted method for the reduction of GO was done by hydrazine which is a very hazardous chemical, both to the human health and to the environment [29]. Employing green reducing agents can therefore act as a highly favorable alternative method for such hazardous materials and for the large-scale production of graphene-like materials. The first green route for the preparation of graphene dispersions from graphite oxide was reported by Fan et al [30]. Previous studies

based on graphene as a filler in various thermosetting resin like epoxy [31-33], polyimide [34, 35], polyurethane [36] showed improvement in mechanical properties.

Studies based on the synthesis and characterizations of phenolic resin/layered silicate nanocomposites were reported earlier [37-41]. Wang and colleagues prepared phenolic resin/surface treated CNT and found that the compressive strength and hardness of the material improved by the incorporation of modified CNT [42]. One of the drawbacks of CNT is their higher production cost which makes it unfavorable for composite preparation. Studies on the morphology and the effect of carbon nanotube filler on tribology of phenol formaldehyde resin based composites are reported elsewhere [43]. Xu and colleagues prepared graphene oxide (GO)/phenol formaldehyde polymer nanocomposites by in situ method [44]. As a result of good dispersion of GO in the polymer matrix and the good interfacial interaction between GO sheets and the polymer matrix resulted in enhancement of thermal stability and mechanical property. A facile in situ synthesis of reduced graphene oxide (RGO) - phenol formaldehyde (PF) composites with an interactive oxidation-reduction reaction was reported by Zhao and co-workers [45]. The presence of π-π stacking interaction and the covalent bond formation between GO and phenol homologs resulted in good dispersion and strong interfacial interaction with the polymer. The results showed enhanced performances in terms of mechanical strength, electrical conductivity, thermal conductivity, and thermal resistance.

In the present study we make use of a highly abundant natural non-toxic bio-material, potato starch, as a very effective reducing agent for the reduction of graphene oxide [46]. The products obtained after reduction is environmentally friendly and reduces the graphene oxide under mild conditions. The importance of the present work is that the incorporation of reduced graphene oxide into the phenol formaldehyde resin and preparation of the nanocomposites without the addition of any curing agents. Heat cure method is adopted for the preparation of the nanocomposites. The resultant

nanocomposites were characterized by microscopic, thermal and mechanical analysis. It is expected that the resultant composites will have potential applications in conductive, thermal interface materials and other high technology industries.

2. Experimental

2.1. Materials

Graphite powder, $NaNO_3$, Conc. H_2SO_4, $KMnO_4$, Hydrogen peroxide, and Ammonia are purchased from Merck, India. Starch potato is procured from LOBA Chemie Pvt. Ltd. Phenol formaldehyde resole resin was purchased from Polyformalin (Ernakulam, Kerala).

2.2. Preparation of the PF/RGO polymer nanocomposites

The reduction of graphene oxide obtained by Hummers method [47] was done by starch potato. The weight percentage of reduced graphene oxide required for the preparation of the polymer nanocomposite was taken on the basis of the solid content of the PF resin. Acetone facilitates the mixing of RGO into the PF matrix. It is then stirred well using a mechanical stirrer with a speed of 4000 rotations/min for 2 h. After stirring, it is sonicated using an ultrasonicator for 1h at a temperature of 60 $^{\circ}$C. Now the sample is transferred into a glass tray containing a glass paper and kept in an oven at a low temperature of 50 $^{\circ}$C until it becomes a semi-cured stage. The sample is then molded in a pre-heated compression molding machine at 100 $^{\circ}$C for 30 min. After cooling, the sheets of polymer nanocomposites were obtained and cut into the required size and can be used for further investigation. The schematic representation of the preparation of PF/RGO nanocomposites is shown in Scheme.1.

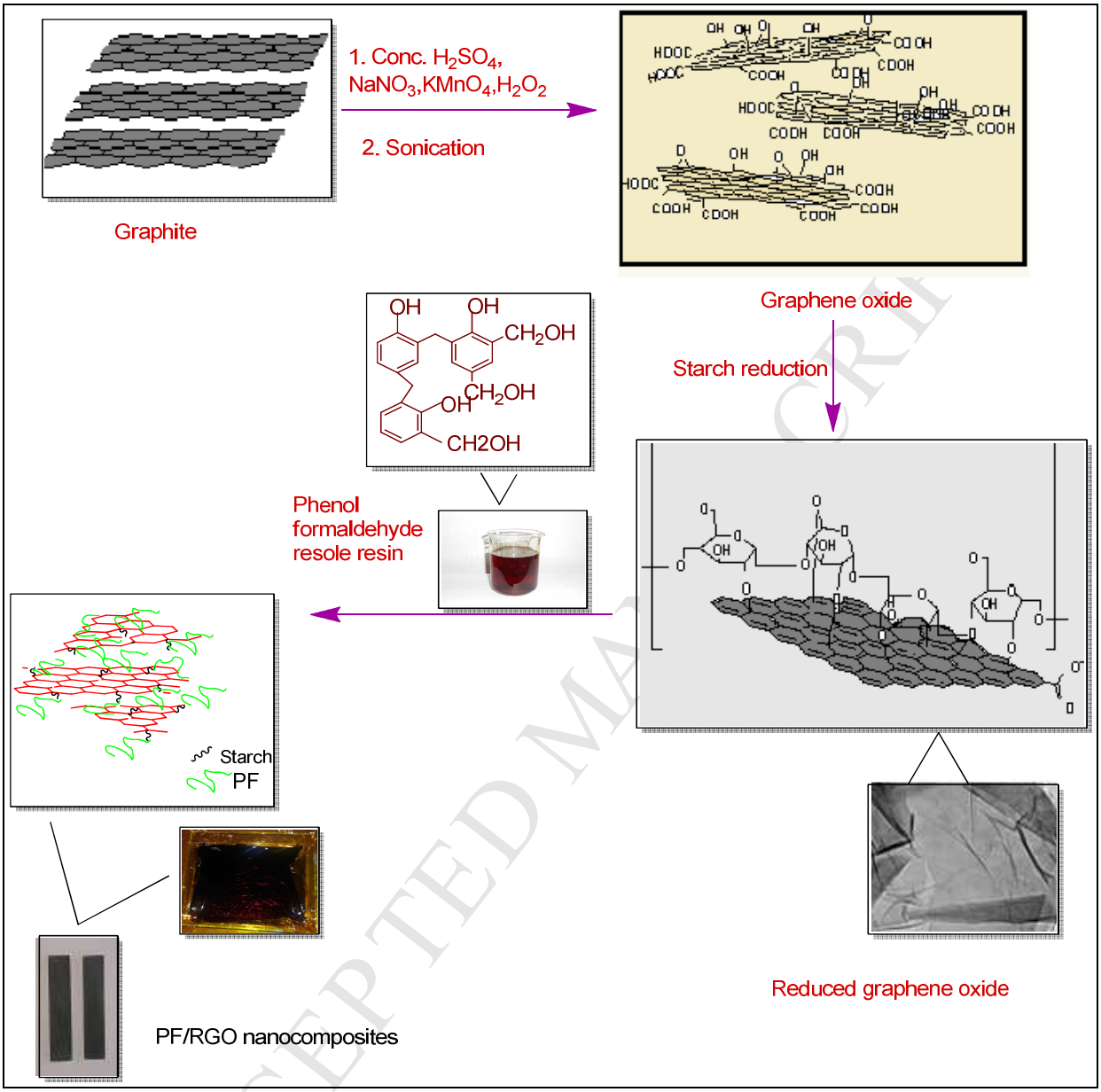

Scheme1. Schematic representation of the preparation of PF/RGO polymer nanocomposite

2.3. Characterization of PF/RGO nanocomposites

2.3.1. Structural characterization

The XRD measurements were done on an X-ray refractometer XPERT-PRO and the intensity was recorded over 2θ angles from 5° to 40° with step size 2θ at 0.001 using a

Ni-filtered Cu K radiation (θ= 1.5406 A^o) and an operating voltage of 45 kV and a filament current of 35 mA. The Raman spectra of the samples were done in WITec Alpha 300 RA confocal Raman microscope with AFM (WITec GmbH, Ulm, Germany).

2.3.2. Morphological characterization

The morphological analysis of the prepared PF/RGO nanocomposites was obtained on a High-Resolution Transmission Electron Microscope JEM-2100HRTEM. The ultra-microtome cutting was employed and collected on a 200 mesh Cu grid for obtaining the TEM images of PF/RGO nanocomposites. WITec Alpha 300 RA confocal Raman microscope with AFM (WITec GmbH, Ulm, Germany) was used to study the AFM image of RGO. The surface morphology of the tensile fractured surfaces of PF/RGO nanocomposites was examined using the Scanning Electron Microscope (JEOL JSM -820 model). To avoid charring during the SEM imaging, the samples are then coated with gold using a vacuum sputter coater.

2.3.3. Mechanical characterization

The tensile properties of the samples were tested using a universal testing machine Tinius Olsen tensile testing machine according to ASTMD 638. The tests were conducted at room temperature for rectangularly shaped samples with a gauge length of 60mm and a crosshead speed of 2mm/min. The impact strength of the notched samples was done by ASTM D256. The Izod impact test is performed for the prepared PF and PF/RGO polymer nanocomposites with Zwick / Roell HIT 25 P model impact tester.

2.3.4. Thermal characterization

Thermal properties of the samples were carried out by using a PerkinElmer STA 6000 (Simultaneous Thermal Analyzer) at a heating rate of 20 ^oC per minute under the nitrogen atmosphere. The amount of the samples used for the analysis was in between 5 and 10 mg and the thermograms were recorded from room temperature to 700 ^oC.

3. Results and discussions

3.1. Property analysis of PF/RGO nanocomposites

The properties of the polymer nanocomposites are depended upon the combined properties of the matrix and filler such as the specific surface area of graphene, interfacial adhesion between the filler and matrix and essential properties of filler and matrix. The properties of graphene sheets such as surface roughness, availability of surface functional groups for attractive interactions, the surface area available for contact with the matrix molecules etc. Therefore it is essential to investigate the morphology of the prepared graphene sheets. Fig.1 (a) and (b) represents the TEM images of RGO sheets. Some scrolling and corrugations are present on the edges of RGO. The RGO nanosheets are layer structured, irregular and folded with lots of wrinkles [48]. The wrinkled morphology of RGO is clearly seen from Fig.5(a) and the layered structure is from Fig.5(b).

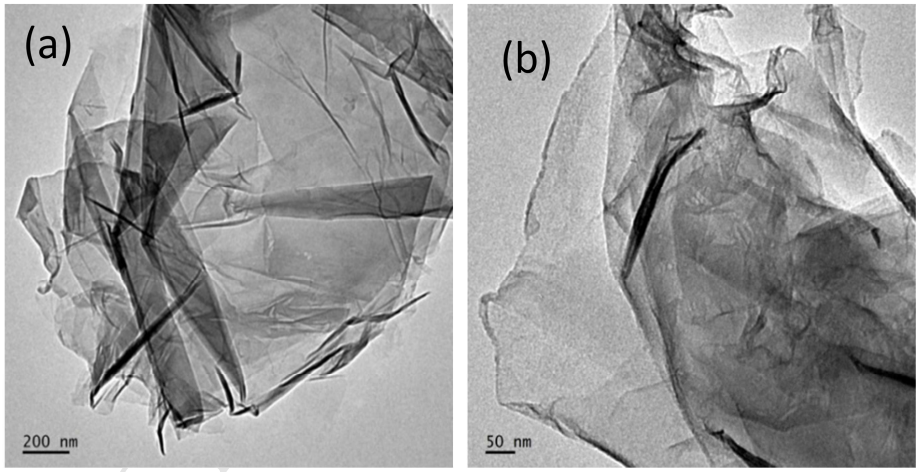

Fig.1. TEM images of RGO in two different magnifications (a) x 200 nm (b) x 50 nm

Fig. 2 shows the AFM image of RGO dispersion in water after deposition on a silicon wafer by drop casting method. The thickness of RGO sheets ranges about 0.67 nm, which are corresponds to the thickness of single layer graphene sheets, observed from the TEM

images (Fig. 1(a) and (b)) and this is due to the removal of most of the hydroxyl, carboxyl and epoxy groups on the surface of GO.

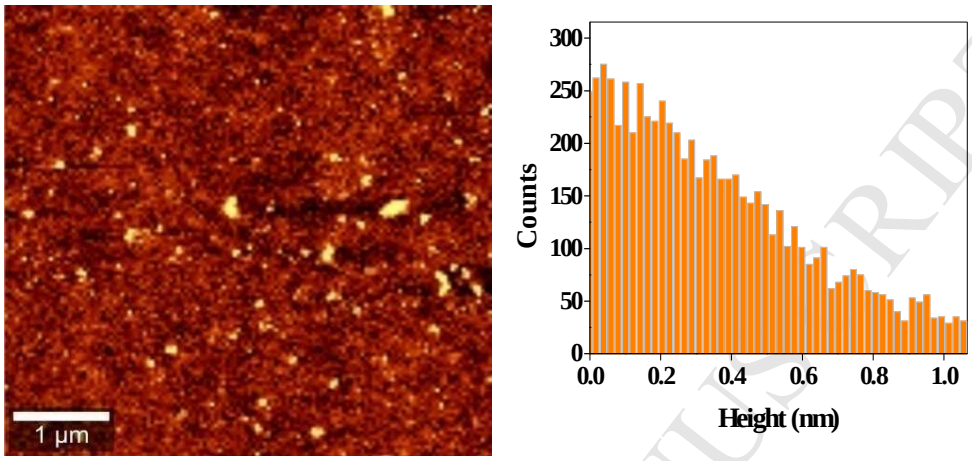

Fig.2. Topographic AFM image and histogram of RGO

32.1. Morphology of PF/RGO nanocomposites

The properties of the nanocomposites strongly depend on the dispersion state of the nanofiller in the polymer matrix. The morphology and dispersion of RGO in PF/RGO nanocomposites observed from the TEM images of 0.12 wt% RGO (which shows higher property improvement) are given in Fig.3. From the figure, it is clear that RGO sheets are homogeneously dispersed in the PF matrix without any large agglomerates. The wrinkled and overlapped RGO sheets are spread throughout the PF matrix as a result of non-covalent interactions (shown in Scheme. 2) between the RGO sheets and PF matrix. Some stacked RGO layers are also observed from the TEM image. On comparing the TEM images of RGO sheets (Fig 1(a) and (b)) with that of PF/RGO composites, it is clear that there was a marked change in the surface morphology of the RGO sheets when it is incorporated into the PF matrix. From this observation, we can conclude that there exists a strong interfacial interaction such as H-bonding and π-π stacking interaction between PF and RGO sheets.

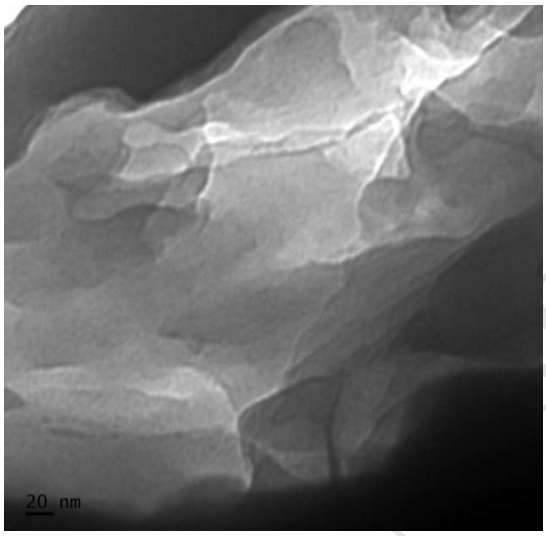

Fig.3.TEM image of 0.12 wt% PF/RGO nanocomposites

3.2.2. XRD analysis

The effects of RGO on the structural properties of nanocomposites studied from the XRD patterns of nanocomposites and are presented in Fig.4. In the case of neat PF, there is no sharp peak observed. The diffraction peak of potato starch reduced graphene oxide is observed around $2\theta = 26.53^{\circ}$ and this peak is totally disappeared in XRD of PF/RGO nanocomposites. The XRD peaks of all PF composites are similar to that of PF. The results suggest that the basal space of reduced graphene oxide changes to an exfoliated morphology in the nanocomposites. Similar results were reported earlier [49]. The XRD result also confirms the reinforcement of RGO into the PF resin and the interfacial interaction with the matrix that affect the crystallization of RGO.

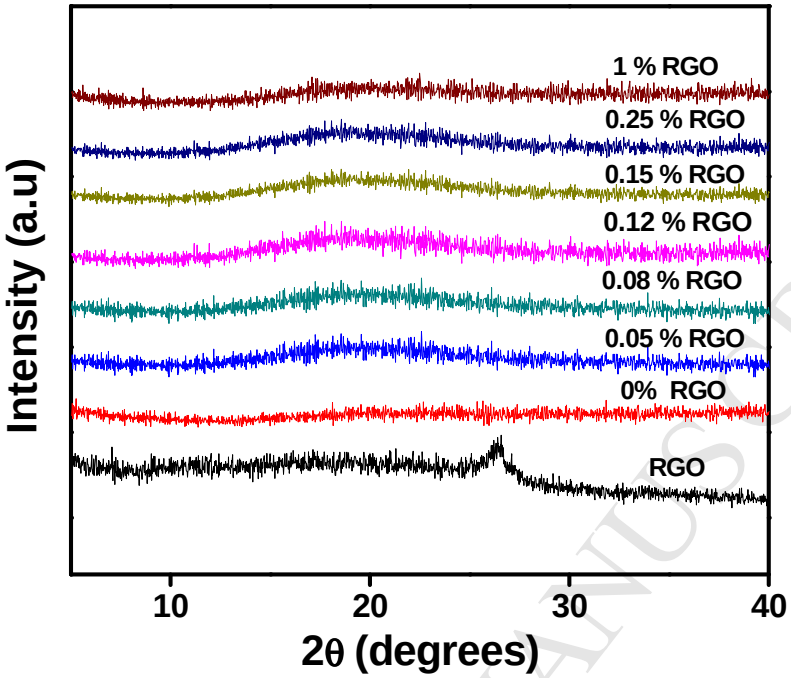

Fig.4. XRD of PF and PF/RGO nanocomposites

3.2.3. Thermal degradation analysis

The degree of thermal stability of the polymer nanocomposites depends on the dispersion, the degree of interaction between filler and matrix, size, shape, nature and amount of filler [50]. The effect of RGO on the thermal properties of PF was studied by TGA analysis and it is shown Fig. 5(a) and 5(b). In the case of neat PF, the initial mass loss is observed below 100 $^{\circ}$C from the DTG graph with a peak temperature of 62.70 $^{\circ}$C. The water absorbed by the powders of cured material before the testing of TGA is evaporated at this temperature range. The weight loss observed below 300 $^{\circ}$C is due to the breakage of the bond between methylene and benzene ring. Above 350 $^{\circ}$C, the polymeric materials undergo gradual disintegration and resulted in the weight loss due to the elimination of certain volatiles. The volatiles usually present are carbon oxides (CO,

CO_2), CH_4, C_2H_6, phenol and its methyl derivatives and also some condensed nuclear hydrocarbons [51]. Above 600 °C, the material undergoes degradation continuously and resulted in the formation of char-like substance. PF/RGO nanocomposites with 0.12 wt% RGO showed higher thermal stability than other wt% of RGO and is due to the good dispersion of RGO in the PF matrix. Better thermal stability of PF/RGO nanocomposites is due to the large surface area of RGO which can provide a good interfacial interaction between RGO and PF matrix. In the study of thermal stability of polymer/clay nanocomposites, clay has two opposing effects like barrier and promoter effects were reported elsewhere [52].

From the TGA results, we found that the RGO sheets exhibit two effects in the thermal stability of PF/RGO nanocomposites, barrier effect and promoter effect. At lower wt% RGO, thermal stability is increased due to the barrier effect and good dispersion of RGO sheets in the PF matrix. However, with the increase in wt% RGO, the promoter effect activates and it increases the degradation of the polymer, thereby decreasing the thermal stability. It is also observed that for 0.25 and 1 wt% PF/RGO the degradation pattern is almost similar to that of RGO, but in the case of 0.12 wt% RGO, the inherent degradation behavior of RGO doesn't affect the PF/RGO nanocomposites.

The temperatures at which 10 and 15% weight loss, the residue at 700 °C and the temperature at which maximum degradation occurred were tabulated in Table 1. It can be seen that at 10% and 15% loss the temperature increases with an increase in wt% RGO. The maximum value of residue at 700 °C is 49.13 and it is observed in 0.12% RGO.

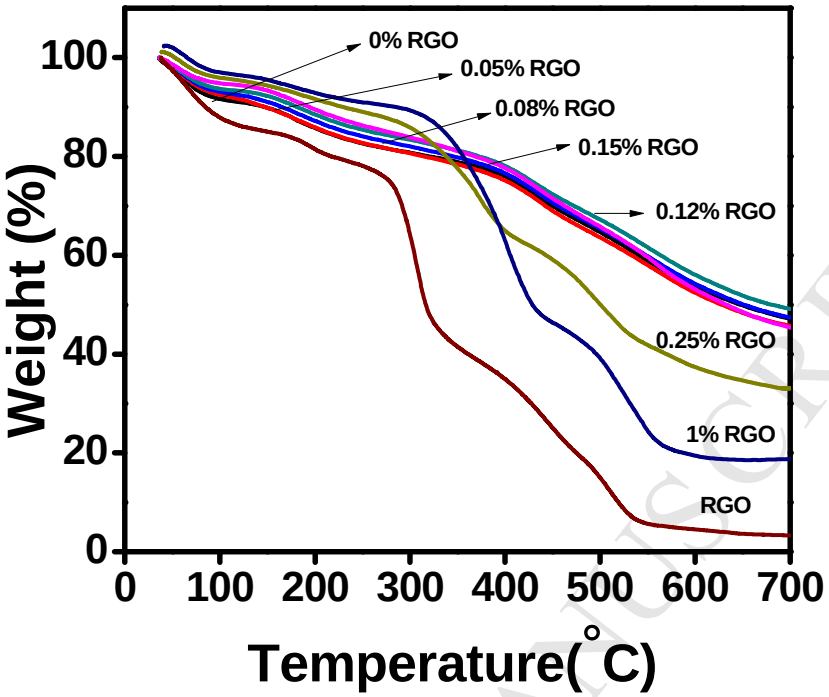

Fig .5 (a) TGA of PF and PF/RGO composites

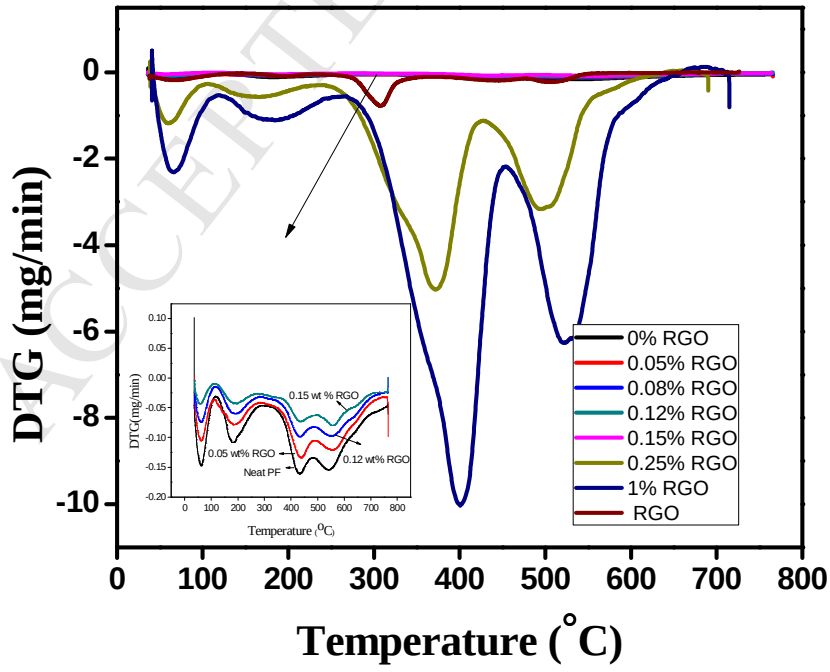

Fig .5 (b) DTG of PF and PF/RGO composites

Table1. Thermal property of PF and PF/RGO composites

Sample	**Temperature (°C) at 10% loss**	**Temperature (°C) at 15% loss**	**Residue at 700 °C**	**Temperature at maximum degradation rate (°C)**
0	147.13	209.85	47.14	429.48
0.05	156.86	219.78	47.30	436.94
0.08	164.84	231.85	47.42	436.94
0.12	180.99	258.73	49.13	432.95
0.15	193.96	257.86	45.39	435.24
0.25	229.59	307.19	33.07	371.92
1	285.42	335.92	18.76	400.31
RGO	84.71	150.80	3.31	308.15

3.2.4. Mechanical Properties of PF/RGO nanocomposites

The mechanical properties of polymer nanocomposites depend on certain factors such as the dispersion of nanofiller in the polymer matrix, alignment of the filler in the matrix, reinforcement phase aspect ratio and interface bonding [53]. The presence of aggregates reduces the effective aspect ratio of the filler. For obtaining effective reinforcement, a strong interfacial adhesion between the nanosheet and polymer matrix is essential. The incompatibility between the phases is the reason for lowering the modulus of the composite. The lowering of modulus can also be due to the low-stress transfer between the polymer matrix and filler. The hydrogen bonds formed between graphene and

polymer matrix also play a crucial role in improving the mechanical property. The H-bonding interaction present during the formation of RGO and PF/RGO nanocomposites is represented in Scheme 2.

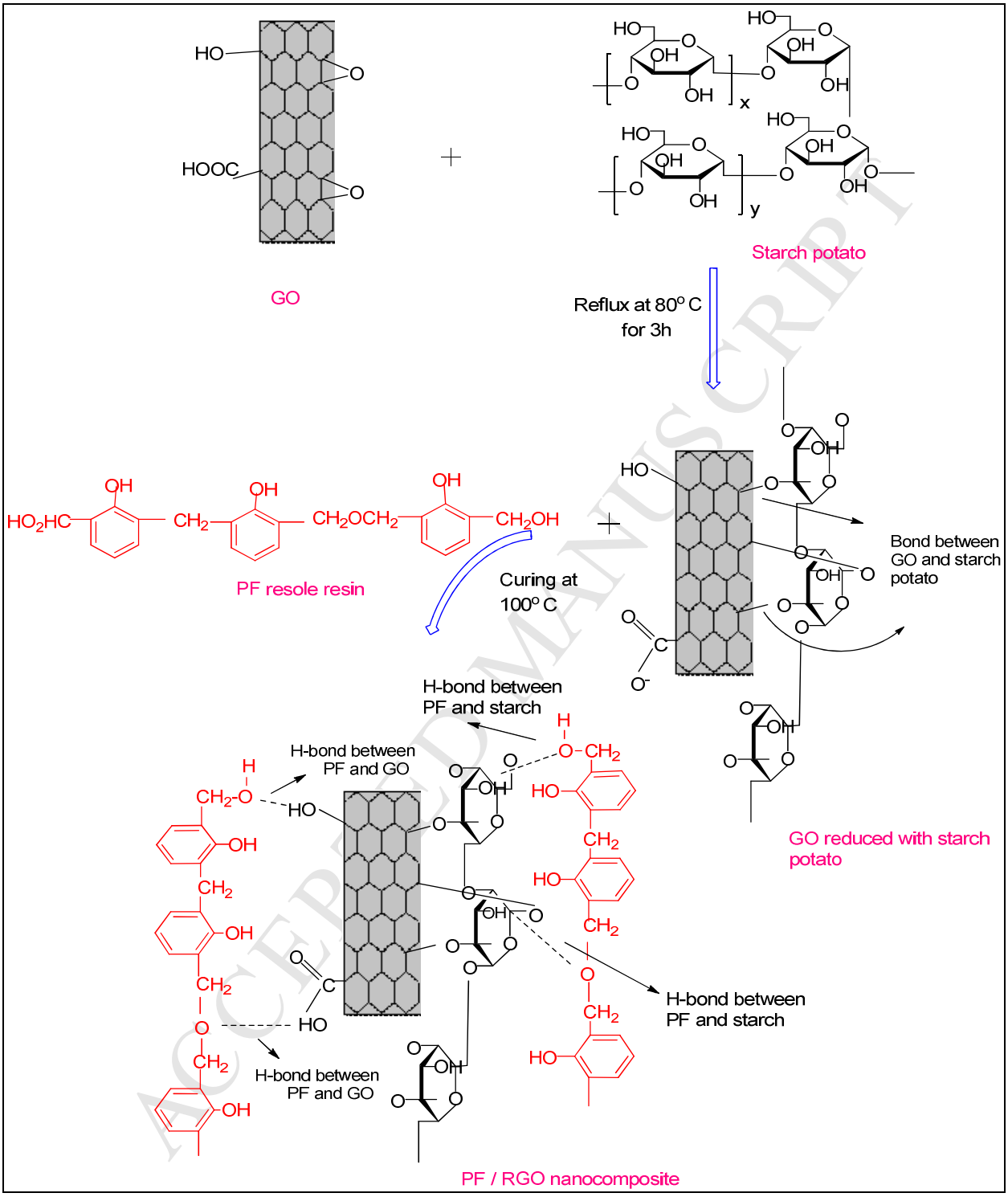

Scheme 2. Schematic representation of interactions present in PF/RGO nanocomposites

With increasing the amount of nanofillers into the polymer matrix, the arrangement of nanosheet in the polymer matrix is expected to be (1) individual dispersion of the nanofiller at intervals in the matrix, (2) side by side joining of the edges of the sheets, (3) overlapping of some parts of the sheets and, (4) the stacking of graphene as layers. When there is an increase in the weight percentage of nanofillers in the polymer matrix, the distance between the layers becomes small and there is a possibility of stacking the layers due to the van der Waals interaction. Like electrical or rheological percolation there is also a mechanical percolation, a critical point of the mechanical properties upon the nanosheet content [54]. There is a good dispersion of nanosheets expected when the amount of the nanofiller lower than this content and also a significant improvement in the mechanical properties is observed. With further loading, the nanosheets get stacked together and as a result, a decrease is observed in mechanical properties.

In the case of graphene nanocomposites, the variations in the mechanical properties are due to the structure and intrinsic properties of the nanofiller graphene, the modifications present on its surface, the nature of the polymer matrix and also the polymerizing processes. The wrinkled morphology of the graphene could enhance the adhesion and mechanical interlocking with the polymer chain. This helps to enhance the interaction and load transfer between the polymer and graphene. According to molecular dynamics and molecular mechanics simulation studies, the mechanical interlocking plays an important role in the interfacial bonding between graphene and polymer matrix. Due to the absorption of the chemical functional groups on the surface of the graphene sheet, the surface roughness of the graphene can strongly interlock with the polymer molecules and arrest the slippage of the polymer chains and thus facilitates the effective load transfer [53]. The mechanical properties of the prepared PF/RGO nanocomposites are summarized in Table 2.

The stress-strain behavior of the neat PF and its nanocomposites with different compositions (0, 0.05, 0.08, 0.12, 0.15, 0.25 and 1wt% RGO) are shown in Fig.6. The PF resin is very brittle and its brittle nature is confirmed from the stress-strain curve. The

stress-strain curve is almost linear to failure in the case of brittle material. This failure occurs before the yield strength is reached. In the case of 0.5 wt% RGO, the amount of filler present in the PF matrix is very low and there is no efficient load transfer between the PF matrix and RGO sheets occur not effectively. For 0.05 wt% RGO, the decrease in the slope of the curve corresponds to the plastic deformation and to microcrack initiation in the matrix. The stress-strain curves of the PF/RGO composites show linear behavior at low strains and the significant change in the slope with a non- linear behavior is observed when the composites undergo complete failure. From the Fig.6, it is clear that the value of tensile stress increases with increasing the RGO content up to 0.12 wt% RGO. The maximum value of tensile stress is observed for composite with 0.12 wt% RGO. This is due to the efficient load transfer between the nanofiller and PF matrix. But when the weight of RGO after 0.15 wt%, the value of stress is found to be decreased and shows a ductile nature. This may due to the aggregation of the RGO content which restricts the load transfer between the layers and results in a decrease in the tensile stress. With the addition of RGO into PF matrix, there are no significant changes produced in the failure pattern, but an improvement in stiffness is observed.

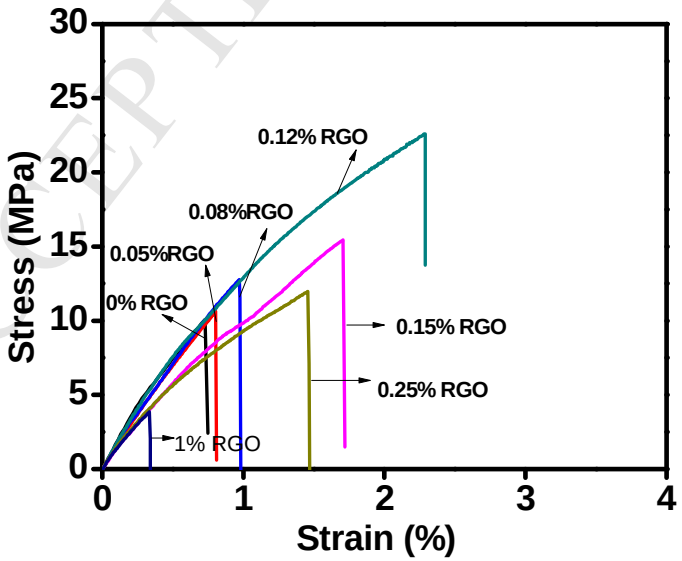

Fig . 6. Stress-strain curves of PF and PF/RGO nanocomposites

The tensile modulus of neat PF and PF/RGO nanocomposites with varying amounts of RGO is as shown in the Fig.7. For neat PF the value of tensile modulus is found to be 1103 MPa. With the incorporation of RGO into the PF matrix, the value of tensile modulus increases to 1675.33 MPa. The increase in the tensile modulus is found to be 34.16% more than the neat PF. There is an increase in tensile modulus is observed from 0.05 wt% RGO to 0.12 wt% RGO. The increase in the modulus of PF/RGO composites is due to the homogeneous dispersion of the RGO into the PF matrix and also the strong interfacial interaction between them. For 0.12 wt% RGO, there is a homogeneous dispersion of the nanofiller in the polymer matrix and also better H-bonding interaction between the functional groups of RGO and PF matrix. There is a good compatibility of the nanofiller into the PF matrix also occurs. The decrease in the modulus value is due to the fact that with increasing amount of RGO in the polymer matrix, there is an aggregation tendency of the RGO sheets in the PF matrix will occur [45].

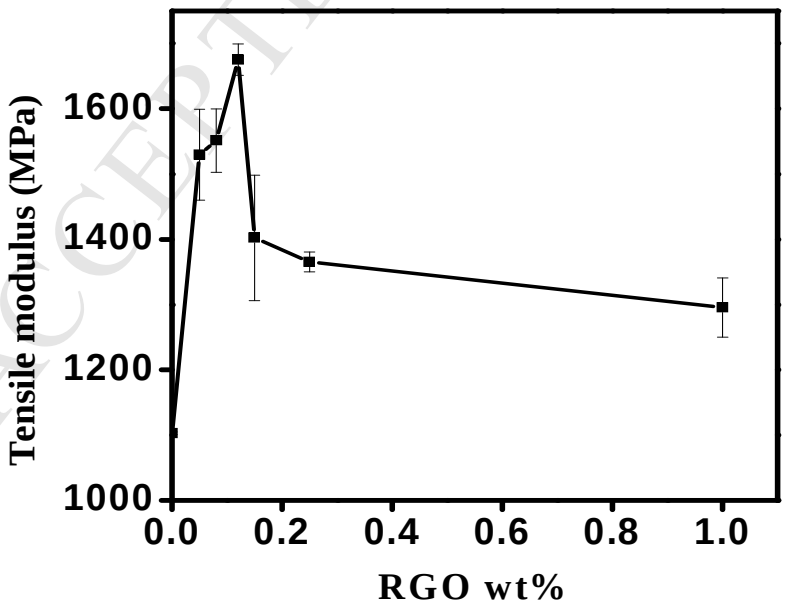

Fig.7. Tensile modulus of PF/RGO polymer nanocomposites

Fig.8 shows the tensile strength of PF nanocomposites with varying wt% of RGO. From the figure, it is clear that the tensile strength of PF/RGO composites shows an increasing trend up to 0.12 wt% RGO. For neat PF, the value of tensile strength is found to be 10.34 MPa and that for 0.05 wt% RGO it is 10.35 MPa. The highest value of tensile strength is 23.5 MPa and it is observed for 0.12 wt% RGO nanocomposite. The increase in the tensile strength compared to neat PF is found to be 55.95% for 0.12 wt% RGO. In the case of high wt% RGO, there occurs a non-homogeneous dispersion of RGO into the PF matrix. With the increased amount of RGO into the PF matrix, there is also a possibility of restacking of layers in the PF matrix occurs and the effective interaction between the RGO and PF matrix gets decreased. These factors lead to a decrease in the mechanical properties of PF/ RGO nanocomposites.

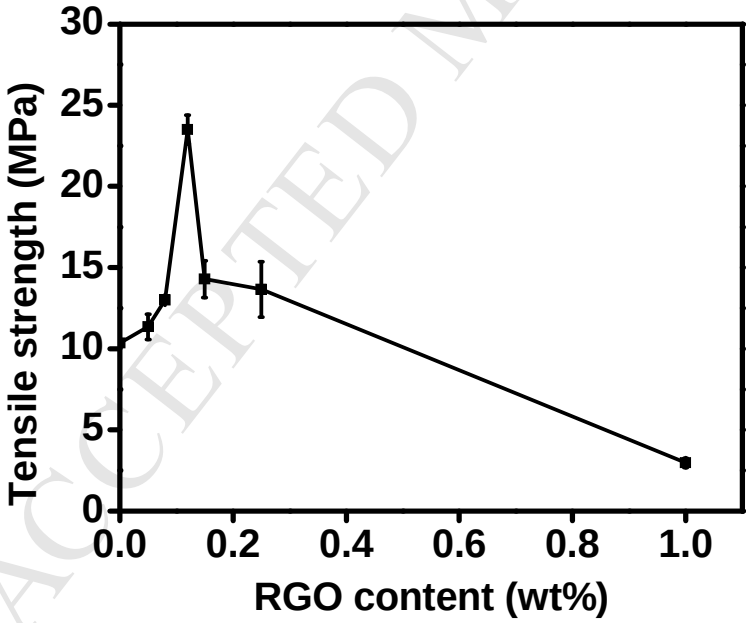

Fig.8. Tensile strength of PF and PF/RGO polymer nanocomposites

The percentage of elongation at break of the PF/RGO nanocomposites shows a decrease due to the high aspect ratio and the interfacial interaction restricts the movement or mobility of the PF molecular chain segments. The values of elongation at break with varying wt% of RGO are shown in Table 2.

Table. 2. Mechanical properties of PF/RGO nanocomposites

RGO contents (%)	**Tensile strength (MPa)**	**Modulus (MPa)**	**Elongation at break (%)**	**Izod Impact Strength (notched) (kJ/m^2)**
0	10.35±0.22	1103±2.00	0.86±0.14	1.12±0.08
0.05	11.35±0.77	1529.66±69.63	1.12±0.05	1.13±0.03
0.08	13.01±0.19	1551.33±48.29	1.16±0.05	1.14±0.09
0.12	23.5±0.90	1675.33±24.05	2.27±0.02	1.23±0.07
0.15	14.29±1.14	1402.25±96.02	1.04±0.35	1.19±0.04
0.25	13.97±1.42	1365.50±15.5	0.9975±0.30	1.17±0.07
1	2.97±0.30	1295.5±45.5	0.8223±0.17	1.13±0.08

4.1. Tensile fracture mechanism

The filler-matrix interaction and the fracture behavior of the nanocomposites can be studied by taking the Scanning Electron Micrographs of the fractured surfaces. Fig. 9(a)-(i) represents the tensile fracture surfaces of neat PF, 0.12 and 1wt% RGO filled PF nanocomposites in three different magnifications. The fracture surface of the neat PF displayed a smooth and orderly surface. The photograph shows the typical brittle fracture of homogeneous thermoset polymers and also indicates its poor resistance to crack initiation and propagation.

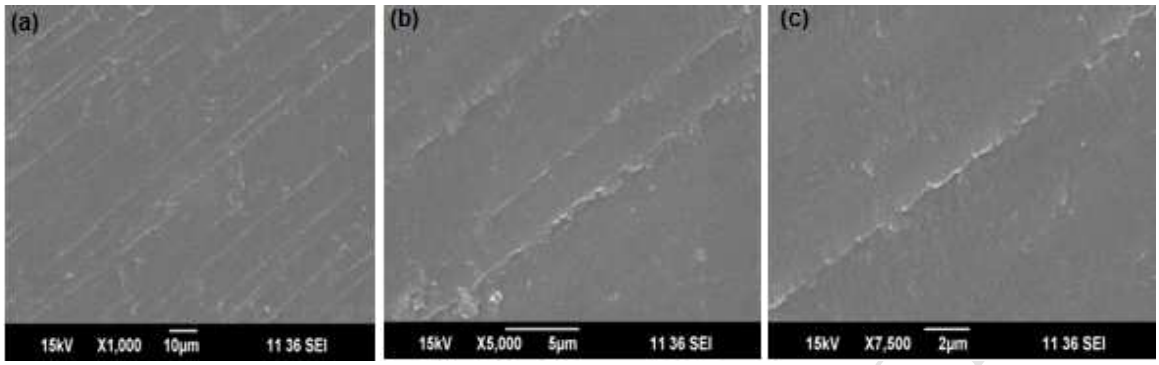

Fig. 9(a) – (c) Scanning electron micrographs of tensile fractured surfaces of neat PF

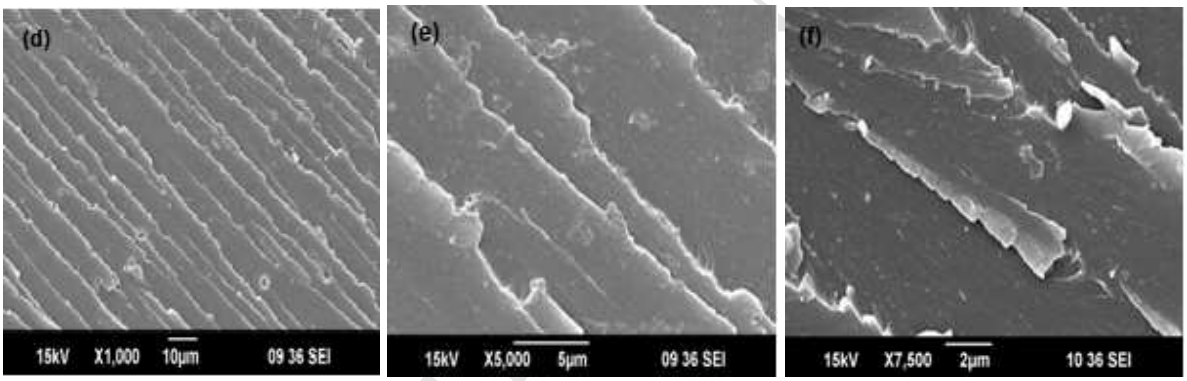

Fig. 9(d) – (f) Scanning electron micrographs of tensile fractured surfaces of PF/ RGO nanocomposites with 0.12 wt % RGO

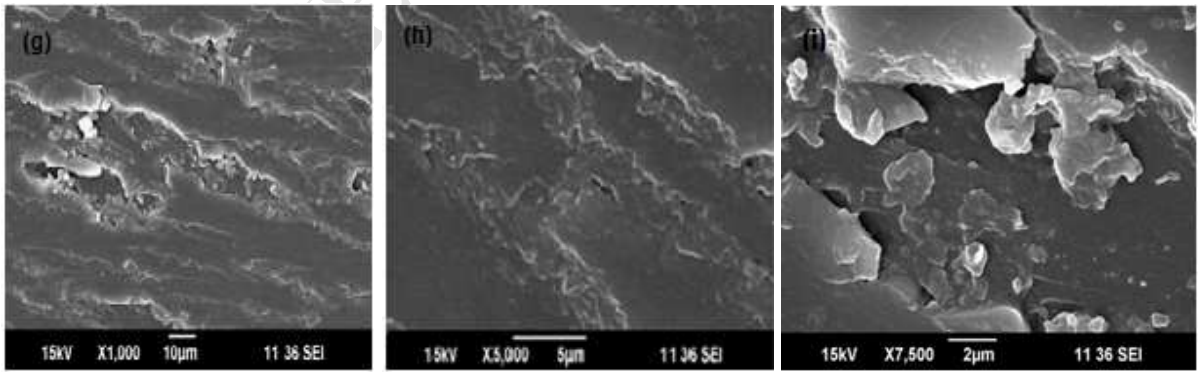

Fig. 9(g) – (i) Scanning electron micrographs of tensile fractured surfaces of PF/ RGO nanocomposites with 1 wt % RGO

In the case of PF nanocomposites with 0.12 wt% RGO the fracture surface shows a quite different morphology. The fracture surface consists of more ridges than the neat PF and the fractured paths are broader. The fracture surface is rougher than the neat PF and more wrinkles are found on it, which indicates the strong interfacial adhesion induced by the surface functional groups of RGO and PF and there is also a good compatibility between them. The presence of more wrinkles actually leads to nanoscale surface roughness which would likely to produce an enhanced mechanical interlocking and adhesion with the polymer chains. Moreover, the strong interfacial bonding also favors the efficient stress transfer from the PF matrix to the RGO sheets and thereby producing an increased mechanical property of the nanocomposites.

The crack initiation and crack growth are expected to be developed in the areas where the nanofillers are present. The presence of such nanofillers generates triaxial stresses above and below the filler particles and restricts shear distortions and thereby encouraging crack initiation. In addition to that, the presence of filler particles that have low surface adhesion to the matrix and separated from the matrix will also generate surface cracks around the particles.

The SEM images of the PF nanocomposites with 1 wt% RGO shows a different morphology of the fracture surface. On analyzing the SEM micrographs it is observed that the presence of agglomeration of RGO sheets and as a result, there is a poor interfacial interaction and poor dispersion between PF matrix and RGO. The image depicts various crack propagation directions on the cleavage surface. The presence of large amounts of RGO sheets creates a 2D hindrance effect on the matrix and that ultimately result in a much coarser fracture surface. The PF/RGO interfacial debonding have a significant contribution to the fracture energy absorption of the nanocompsite when there is a low content of RGO in the PF matrix. The interfacial adhesion arising from the noncovalent debonding mechanisms such as hydrogen bonding and π-π interactions are operating and are considered as the causes of debonding.

4.2. Theoretical modeling of tensile properties

The most widely used theoretical modeling for the determination of tensile modulus of nanocomposites with graphene that is distributed in random or unidirectional is Halpin – Tsai model [55, 56]. The modified form of Halpin- Tsai equation for graphene sheets that are arranged randomly in the polymer matrix is

$$E_r = \left[\frac{3}{8}\frac{1+\left(\frac{2l_g}{3t_g}\right)\eta_L V_g}{1-\eta_L V_g} + \frac{5}{8}\frac{1+2\eta_T V_g}{1-\eta_T V_g}\right]E_p \quad (1)$$

where

$$\eta_L = \frac{(E_g/E_p)-1}{(E_g/E_p)+(2l_g/3t_g)} \quad (2)$$

$$\eta_T = \frac{(E_g/E_p)-1}{(E_g/E_p)+2} \quad (3)$$

For unidirectional (parallel) arranged graphene the modified Halpin- Tsai equation is

$$E_{||} = \left[\frac{1+(2l_g/3t_g)\eta_L V_g}{1-\eta_L V_g}\right]E_p \quad (4)$$

where E_r, E_g and E_p are Young's modulus of the nanocomposite, graphene, and polymer respectively. The Young's modulus of PF is 1.03GPa, obtained from the experiment and that of free-standing monolayer graphene is ~ 1TPa [56]. The length, thickness and volume fraction of the graphene are l_g, t_g and V_g respectively. The thickness and average length of RGO are 0.67 nm and 1.05 nm from the AFM image (Fig.2). Fig.10 shows the comparison of experimental obtained tensile modulus with theoretical value and it is clear that the experimental and theoretical values are in very good agreement for low volume percentages of filler. The experimentally calculated values are close to randomly dispersed RGO. But at higher volume % RGO, the experimental values are lower than the theoretical value, reveals the restacking of RGO layers in the composites.

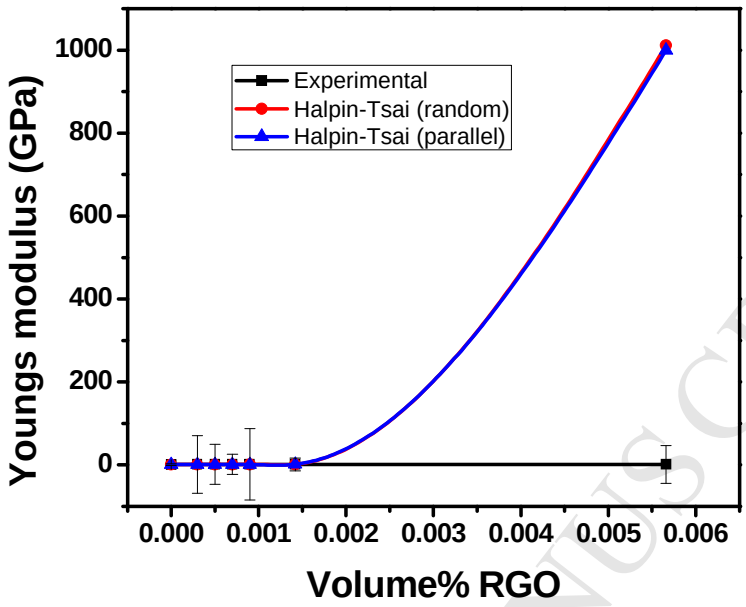

Fig.10. Theoretical modeling of the tensile modulus of PF/ RGO nanocomposites

4.3. The Impact strength of PF/RGO nanocomposites

Impact tests are very useful in understanding the toughness of the material. The toughness of a material is its ability to absorb energy during plastic deformation. In the case of brittle materials, toughness is low due to the small amount of plastic deformation that they can endure. The factors that affect the impact strength of materials are notched, temperature, yield strength, and ductility, fracture mechanism, size of the specimen etc. The shape and size of the filler also affect the properties of the nanocomposites. Fig.11 shows the Izod impact strength of RGO filled PF polymer nanocomposites. In the case of RGO filled nanocomposites, the impact strength increases with increasing the RGO content and 0.12 wt% show the maximum value of impact strength which is 9% more than that of neat PF.

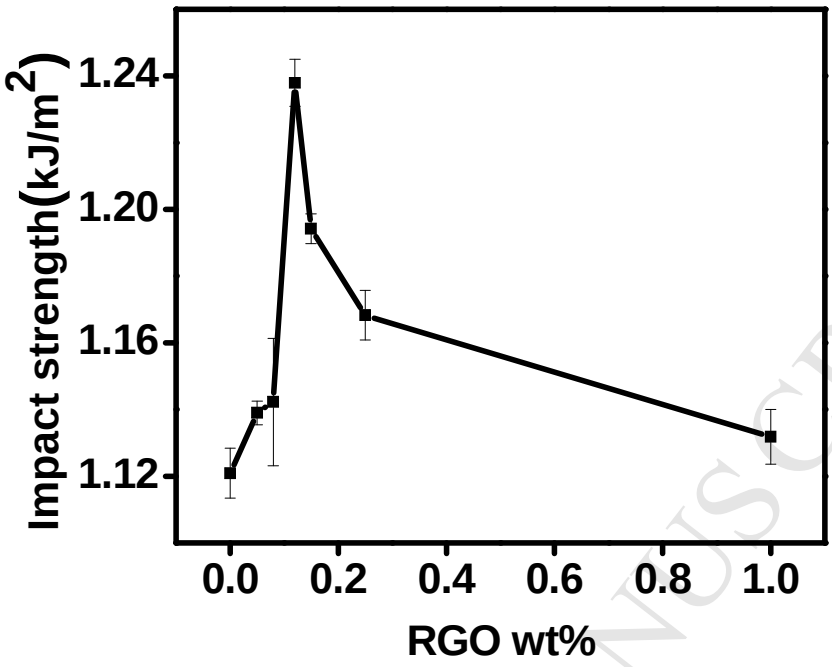

Fig.11. Impact strength of PF/RGO nanocomposites

5. Conclusions

We prepared PF/RGO nanocomposites successfully and studied their mechanical and thermal properties. The RGO sheets used for the preparation of nanocomposites were obtained by the reduction of graphene oxide by a mild natural reducing agent potato starch. The TEM images confirmed the wrinkled and layered nature of RGO. From AFM images, the measured thickness of RGO is in nanometer scale. XRD results of the nanocomposites confirmed the successful incorporation of RGO into the PF matrix. The thermal stability of the prepared nanocomposites is studied by TGA and showed that with increasing wt % of RGO there is an increase in thermal stability of the PF/RGO polymer nanocomposites up to 0.12 wt% RGO and decreases at higher wt% RGO. 0.12 wt% RGO shows high thermal stability due to good dispersion and interfacial interaction between PF and RGO. The mechanical properties of PF/RGO nanocomposites increased with increase in RGO content up to 0.12 wt%. Moreover, the tensile strength, tensile modulus

and impact strength of PF/RGO nanocomposites increase by 56, 34 and 9% respectively as compared to that of neat PF. The SEM images of the tensile fracture surface give the difference in the morphology of nanocomposites with good dispersion and aggregates of RGO compared with neat PF. There is a very good agreement with theoretically and experimentally calculated values of tensile modulus of PF/RGO nanocomposites at lower wt% RGO and the sheets are oriented in the PF matrix randomly.

Acknowledgements

The authors are grateful to the financial support under DST-FIST (No. 487/DST/FIST/15-16) New Delhi to Sree Sankara College, Kalady.

References

1. Pilato L. Phenolic resins: 100 Years and still going strong. React Funct Polym 2013;73:270–7. doi:10.1016/j.reactfunctpolym.2012.07.008.
2. Rafiee MA, Rafiee J, Srivastava I, Wang Z, Song H, Yu ZZ, et al. Fracture and fatigue in graphene nanocomposites. Small 2010;6:179–83. doi:10.1002/smll.200901480.
3. Mylvaganam K, Zhang L. In Situ Polymerization on Graphene Surfaces. J Phys Chem C 2013;117:2817–23. doi:10.1021/jp310312g.
4. Balasubramanyan S, Sasidharan S, Poovathinthodiyil R, Ramakrishnan RM, Narayanan BN. Sucrose-mediated mechanical exfoliation of graphite: A green method for the large scale production of graphene and its application in catalytic reduction of 4-nitrophenol. New J Chem 2017;41:11969–78. doi:10.1039/c7nj01900a.
5. Luo B, Gao E, Geng D, Wang H, Xu Z, Yu G. Etching-Controlled Growth of Graphene by Chemical Vapor Deposition. Chem Mater 2017;29:1022–7. doi:10.1021/acs.chemmater.6b03672.
6. Pei S, Wei Q, Huang K, Cheng H, Ren W. Green synthesis of graphene oxide by seconds timescale water electrolytic oxidation. Nat Commun n.d.:1–9. doi:10.1038/s41467-017-02479-z.
7. Dong L, Yang J, Chhowalla M, Loh KP. Synthesis and reduction of large sized graphene oxide sheets. Chem Soc Rev 2017;46:7306–16. doi:10.1039/c7cs00485k.
8. Torres D, Pinilla JL, Suelves I. Unzipping of multi-wall carbon nanotubes with different diameter distributions: Effect on few-layer graphene oxide obtention. Appl Surf Sci 2017;424:101–10. doi:10.1016/j.apsusc.2017.01.273.

9. Qin B, Zhang T, Chen H, Ma Y. The growth mechanism of few-layer graphene in the arc discharge process. Carbon N Y 2016;102:494–8. doi:10.1016/j.carbon.2016.02.074.
10. Stankovich S, Dikin DA, Piner RD, Kohlhaas KA, Kleinhammes A, Jia Y, et al. Synthesis of graphene-based nanosheets via chemical reduction of exfoliated graphite oxide. Carbon N Y 2007;45:1558–65. doi:10.1016/J.CARBON.2007.02.034.
11. Tung VC, Allen MJ, Yang Y, Kaner RB. High-throughput solution processing of large-scale graphene. Nat Nanotechnol 2009;4:25–9. doi:10.1038/nnano.2008.329.
12. Li D, Müller MB, Gilje S, Kaner RB, Wallace GG. Processable aqueous dispersions of graphene nanosheets. Nat Nanotechnol 2008;3:101–5. doi:10.1038/nnano.2007.451.
13. Park S, An J, Jung I, Piner RD, An SJ, Li X, et al. Colloidal Suspensions of Highly Reduced Graphene Oxide in a Wide Variety of Organic Solvents. Nano Lett 2009;9:1593–7. doi:10.1021/nl803798y.
14. Pham VH, Cuong TV, Hur SH, Shin EW, Kim JS, Chung JS, et al. Fast and simple fabrication of a large transparent chemically-converted graphene film by spray-coating. Carbon N Y 2010;48:1945–51. doi:10.1016/j.carbon.2010.01.062.
15. Villar-Rodil S, Paredes JI, Martínez-Alonso A, Tascón JMD. Preparation of graphene dispersions and graphene-polymer composites in organic media. J Mater Chem 2009;19:3591. doi:10.1039/b904935e.
16. Pham VH, Cuong TV, Nguyen-Phan TD, Pham HD, Kim EJ, Hur SH, et al. One-step synthesis of superior dispersion of chemically converted graphene in organic solvents. Chem Commun 2010;46:4375–7. doi:10.1039/c0cc00363h.
17. Si Y, Samulski ET. Synthesis of Water Soluble Graphene. Nano Lett 2008;8:1679–82. doi:10.1021/nl080604h.
18. Muszynski R, Seger B, Kamat P V. Decorating Graphene Sheets with Gold Nanoparticles. J Phys Chem C 2008;112:5263–6. doi:10.1021/jp800977b.
19. Wang G, Yang J, Park J, Gou X, Wang B, Liu H, et al. Facile Synthesis and Characterization of Graphene Nanosheets. J Phys Chem C 2008;112:8192–5. doi:10.1021/jp710931h.
20. Moon IK, Lee J, Ruoff RS, Lee H. Reduced graphene oxide by chemical graphitization. Nat Commun 2010;1:1–6. doi:10.1038/ncomms1067.
21. Pham HD, Pham VH, Cuong TV, Nguyen-Phan T-D, Chung JS, Shin EW, et al. Synthesis of the chemically converted graphene xerogel with superior electrical conductivity. Chem Commun 2011;47:9672. doi:10.1039/c1cc13329b.

22. Pei S, Zhao J, Du J, Ren W, Cheng H-M. Direct reduction of graphene oxide films into highly conductive and flexible graphene films by hydrohalic acids. Carbon N Y 2010;48:4466–74. doi:10.1016/J.CARBON.2010.08.006.
23. Chen W, Yan L, Bangal PR. Chemical Reduction of Graphene Oxide to Graphene by Sulfur-Containing Compounds. J Phys Chem C 2010;114:19885–90. doi:10.1021/jp107131v.
24. Fan Z, Wang K, Wei T, Yan J, Song L, Shao B. An environmentally friendly and efficient route for the reduction of graphene oxide by aluminum powder. Carbon N Y 2010;48:1686–9. doi:10.1016/J.CARBON.2009.12.063.
25. Fan Z-J, Kai W, Yan J, Wei T, Zhi L-J, Feng J, et al. Facile Synthesis of Graphene Nanosheets *via* Fe Reduction of Exfoliated Graphite Oxide. ACS Nano 2011;5:191–8. doi:10.1021/nn102339t.
26. Mei X, Ouyang J. Ultrasonication-assisted ultrafast reduction of graphene oxide by zinc powder at room temperature. Carbon N Y 2011;49:5389–97. doi:10.1016/j.carbon.2011.08.019.
27. Liu Y, Li Y, Zhong M, Yang Y, Yuefang Wen, Wang M. A green and ultrafast approach to the synthesis of scalable graphene nanosheets with Zn powder for electrochemical energy storage. J Mater Chem 2011;21:15449. doi:10.1039/c1jm12599k.
28. Zhou X, Zhang J, Wu H, Yang H, Zhang J, Guo S. Reducing Graphene Oxide via Hydroxylamine: A Simple and Efficient Route to Graphene. J Phys Chem C 2011;115:11957–61. doi:10.1021/jp202575j.
29. Paredes JI, Villar-Rodil S, Fernández-Merino MJ, Guardia L, Martínez-Alonso A, Tascón JMD. Environmentally friendly approaches toward the mass production of processable graphene from graphite oxide. J Mater Chem 2011;21:298–306. doi:10.1039/c0jm01717e.
30. Fan X, Peng W, Li Y, Li X, Wang S, Zhang G, et al. Deoxygenation of Exfoliated Graphite Oxide under Alkaline Conditions: A Green Route to Graphene Preparation. Adv Mater 2008;20:4490–3. doi:10.1002/adma.200801306.
31. Feng H, Wang X, Wu D. Fabrication of Spirocyclic Phosphazene Epoxy-Based Nanocomposites with Graphene via Exfoliation of Graphite Platelets and Thermal Curing for Enhancement of Mechanical and Conductive Properties. Ind Eng Chem Res 2013;52:10160–71. doi:10.1021/ie400483x.
32. Bao C, Guo Y, Song L, Kan Y, Qian X, Hu Y. In situ preparation of functionalized graphene oxide/epoxy nanocomposites with effective reinforcements. J Mater Chem 2011;21:13290. doi:10.1039/c1jm11434d..
33. Chandrasekaran S, Seidel C, Schulte K. Preparation and characterization of graphite nano-platelet (GNP)/ epoxy nano-composite : Mechanical , electrical

and thermal properties. Eur Polym J 2013;49:3878–88. doi:10.1016/j.eurpolymj.2013.10.008.

34. Chen D, Zhu H, Liu T. In Situ Thermal Preparation of Polyimide Nanocomposite Films Containing Functionalized Graphene Sheets. ACS Appl Mater Interfaces 2010;2. doi:10.1021/am1008437.
35. Ha HW, Choudhury A, Kamal T, Kim D, Park S. Effect of Chemical Modification of Graphene on Mechanical, Electrical, and Thermal Properties of Polyimide/Graphene Nanocomposites. ACS Appl Mater Interfaces 2012;4:4623–30. doi:10.1021/am300999g.
36. Kim JT, Kim BK, Kim EY, Kwon SH, Jeong HM. Synthesis and properties of near IR induced self-healable polyurethane/graphene nanocomposites. Eur Polym J 2013;49:3889–96. doi:10.1016/j.eurpolymj.2013.10.009.
37. Wang D-C, Chang G-W, Chen Y. Preparation and thermal stability of boron-containing phenolic resin/clay nanocomposites. Polym Degrad Stab 2008;93:125–33. doi:10.1016/j.polymdegradstab.2007.10.021.
38. Wu Z, Zhou C, Qi R. The preparation of phenolic resin/montmorillonite nanocomposites by suspension condensation polymerization and their morphology. Polym Compos 2002;23:634–46. doi:10.1002/pc.10463.
39. Kaynak C, Tasan CC. Effects of production parameters on the structure of resol type phenolic resin/layered silicate nanocomposites. Eur Polym J 2006;42:1908–21. doi:10.1016/j.eurpolymj.2006.03.008.
40. Choi MH, Chung IJ, Lee JD. Morphology and Curing Behaviors of Phenolic Resin-Layered Silicate Nanocomposites Prepared by Melt Intercalation. Chem Mater 2000;12:2977–83. doi:10.1021/cm000227t.
41. Byun HY, Choi MH, Chung IJ. Synthesis and Characterization of Resol Type Phenolic Resin/Layered Silicate Nanocomposites. Chem Mater 2001;13:4221–6. doi:10.1021/cm0102685.
42. Wang H, Lu R, Huang Z, Huang T, Cong P, Li T. Effect of Surface-Treated Carbon Nanotubes on the Mechanical and Tribological Performances of Phenolic Resin. J Macromol Sci Part B 2012;51:1148–58. doi:10.1080/00222348.2011.625905.
43. Igarashi A, Terasawa T, Kanie M, Yamanobe T, Komoto T. A Morphological Study of the Effect of Carbon Nanotube Filler on Tribology of Phenol/Formaldehyde Resin-based Composites. Polym J 2005;37:522–8. doi:10.1295/polymj.37.522.
44. Xu W, Wei C, Lv J, Liu H, Huang X, Liu T. Preparation, Characterization, and Properties of In Situ Formed Graphene Oxide/Phenol Formaldehyde Nanocomposites. J Nanomater 2013;2013:1–6. doi:10.1155/2013/319840.

45. Zhao X, Li Y, Wang J, Ouyang Z, Li J, Wei G, et al. Interactive Oxidation–Reduction Reaction for the in Situ Synthesis of Graphene–Phenol Formaldehyde Composites with Enhanced Properties. ACS Appl Mater Interfaces 2014;6:4254–63. doi:10.1021/am405983a.
46. Feng Y, Feng N, Du G. A green reduction of graphene oxide via starch-based materials. RSC Adv 2013;3:21466. doi:10.1039/c3ra43025a.
47. Hummers WS, Offeman RE. Preparation of Graphitic Oxide. J Am Chem Soc 1958;80:1339–1339. doi:10.1021/ja01539a017.
48. Sandhya PK, Jose J, Sreekala MS, Padmanabhan M, Kalarikkal N, Thomas S. Reduced graphene oxide and ZnO decorated graphene for biomedical applications. Ceram Int 2018;44:15092–8. doi:10.1016/j.ceramint.2018.05.143.
49. Sabagh S, Aref Azar A, Bahramian AR. High temperature ablation and thermo-physical properties improvement of carbon fiber reinforced composite using graphene oxide nanopowder. Compos Part A Appl Sci Manuf 2017;101:326–33. doi:10.1016/j.compositesa.2017.07.001.
50. Bikiaris D. Can nanoparticles really enhance thermal stability of polymers? Part II: An overview on thermal decomposition of polycondensation polymers. Thermochim Acta 2011;523:25–45. doi:10.1016/j.tca.2011.06.012.
51. Si J, Li J, Wang S, Li Y, Jing X. Enhanced thermal resistance of phenolic resin composites at low loading of graphene oxide. Compos Part A Appl Sci Manuf 2013;54:166–72. doi:10.1016/j.compositesa.2013.07.019.
52. Chrissafis K, Bikiaris D. Can nanoparticles really enhance thermal stability of polymers? Part I: An overview on thermal decomposition of addition polymers. Thermochim Acta 2011;523:1–24. doi:10.1016/j.tca.2011.06.010.
53. Galpaya D, Wang M, Liu M, Motta N, Waclawik E, Yan C. Recent Advances in Fabrication and Characterization of Graphene-Polymer Nanocomposites. Graphene 2012;01:30–49. doi:10.4236/graphene.2012.12005.
54. Zhao X, Zhang Q, Chen D, Lu P. Enhanced Mechanical Properties of Graphene-Based Poly(vinyl alcohol) Composites. Macromolecules 2010;43:2357–63. doi:10.1021/ma902862u.
55. Choudhury A. Preparation and characterization of nanocomposites of poly-p-phenylene benzobisthiazole with graphene nanosheets. RSC Adv 2014;4:8856. doi:10.1039/c3ra46908e.
56. Ma H-L, Zhang Y, Hu Q-H, He S, Li X, Zhai M, et al. Enhanced mechanical properties of poly(vinyl alcohol) nanocomposites with glucose-reduced graphene oxide. Mater Lett 2013;102–103:15–8. doi:10.1016/j.matlet.2013.03.094.